Multimodal gradients across mouse cortex

Ben D. Fulcher[a], John D. Murray[b], Valerio Zerbi[c], and Xiao-Jing Wang[d,e]

[a]School of Physics, Sydney University, Sydney, NSW 2006, Australia
[b]Department of Psychiatry, Yale University School of Medicine, New Haven, CT, USA
[c]Neural Control of Movement Lab, D-HEST, ETH Zürich, Winterthurerstrasse 190, 8057 Zürich, Switzerland
[d]Center for Neural Science, New York University, 4 Washington Place, New York, NY 10003, USA
[e]Key Laboratory of Brain Functional Genomics and Institute of Cognitive Neuroscience, East China Normal University, Shanghai 200062, China

The primate cerebral cortex displays a hierarchical organization that extends from primary sensorimotor to association areas, supporting increasingly integrated function that is underpinned by a gradient of heterogeneity in the brain's microcircuits. The extent to which these properties of brain organization are unique to primate or may be conserved across mammals remains unknown. Here we report the topographic similarity of large-scale gradients in cytoarchitecture, brain-related gene expression, interneuron cell densities, and long-range axonal connectivity, which vary from primary sensory through to prefrontal areas of mouse cortex, highlighting an underappreciated spatial dimension of mouse cortical specialization. Using the T1w:T2w magnetic resonance imaging (MRI) map as a common spatial reference for comparison across species, we report interspecies agreement in a range of cortical gradients, including a significant correspondence between gene transcriptional maps in mouse cortex with their human orthologs in human cortex. The interspecies correspondence of large-scale cortical gradients suggests that a conserved anatomical organization may underlie hierarchical specialization in mammalian brains.

neuroscience | mouse | cortical hierarchy | gene expression

Correspondence: ***ben.fulcher@sydney.edu.au & xjwang@nyu.edu***

The cellular makeup of cortical microcircuits, including their cyto-, myelo-, and synaptic architecture, varies across the brain (1–5) as macroscopic spatial gradients (6–9). Variations in cortical microcircuits along a hierarchical gradient of increasing functional integration, from primary sensory to transmodal association areas (10), may underlie the corresponding functional specialization (11). The extent to which hierarchical organization represents a common mammalian organizational principle is unclear. For example, while the structural hierarchy of feedforward and feedback connections in macaque display relatively consistent laminar profiles (12), intracortical mouse projections display more diverse laminar patterning (13). Furthermore, the high level of cortical differentiation between primary sensory and frontal areas in monkey is absent in the relatively homogeneous mouse cortex (14–16). The degree to which mouse cortex displays large-scale hierarchical gradients, and the extent to which they match corresponding variation in primate cortex thus remains unknown.

The mouse is an ideal model to investigate gradients of cortical microstructure, with experimental datasets from diverse modalities available in standardized anatomical reference spaces (17). Cortical maps of a wide range of properties, many of which are unavailable in human, have already been measured in mouse, including: (i) gene expression with approximate genome-wide coverage (18), (ii) interneuron cell densities (19), (iii) tract-traced axonal connectivity (13, 20–23), (iv) cytoarchitecture (24), (v) cell/neuron density (25, 26), and (vi) resting-state fMRI (27–29). Existing work has demonstrated an association between pairs of these measurements (28–30) but—with the notable exception of an analysis of interareal differences in the relative densities of GABAergic neuron subtypes (19)—these data have not previously been characterized together from the viewpoint of macroscopic gradients.

The noninvasive MRI measurement, the T1w:T2w ratio, has been measured in mouse, macaque, and human, providing a common reference for linking large-scale gradients across species. In macaque cortex, T1w:T2w varies along the structural hierarchy of feedforward-feedback projections, and in human cortex it follows dominant gene transcriptional gradients (11), positioning as a strong candidate marker of hierarchical specialization. Here we show for the first time that gradients of diverse properties of mouse cortex exhibit a common spatial patterning along a candidate functional hierarchy. Using T1w:T2w as a common reference, we further demonstrate a correspondence of gradients of cytoarchitecture between mouse, macaque and human, and with transcriptional maps of ortholog genes between mouse and human. Our results point to a common principle of cortical heterogeneity that may underlie the functional specialization of mammalian cortical circuits.

Results

We analyzed the spatial maps of diverse cortical properties across 40 areas of the Allen Reference Atlas (ARA) (31), shown in Figs 1A,B. The similarity between two spatial maps was quantified as the Spearman rank correlation coefficient, ρ, across as many cortical areas as could be matched between a given pair of modalities (40 unless otherwise specified).

Cortical gradients follow T1w:T2w. We first investigated whether the T1w:T2w map is informative of functionally relevant macroscopic gradients of cortical variation in mouse, as it is in macaque and human (11). As shown in Fig. 1A, the T1w:T2w map of the mouse cortex displays non-trivial anatomical specificity on top of a broad spatial embedding: increasing along the inferior–superior axis, $|\rho| = 0.53$ ($p = 5 \times 10^{-4}$; see Supporting Information), perhaps in part reflecting a neurodevelopmental gradient of cortical maturation (32). As shown in Fig. 1B, T1w:T2w broadly decreases across five spatially-localized connectivity modules (13), from somatomotor to prefrontal areas, consistent with

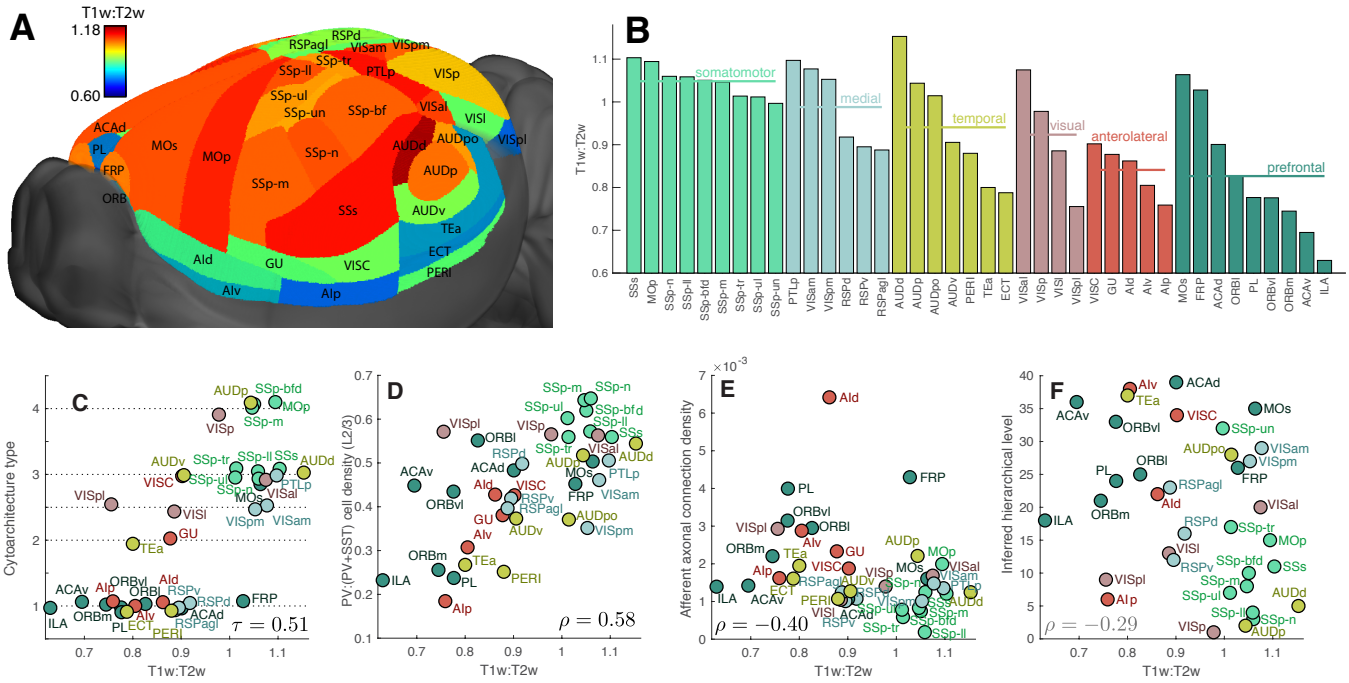

Fig. 1. The spatial map of the MRI measurement, T1w:T2w, is correlated with diverse structural properties. A Variation in T1w:T2w across mouse cortical areas. **B** T1w:T2w broadly decreases across families of connectivity-based groupings of cortical areas (13), from somatomotor areas through to anterolateral and prefrontal areas. Groups are ordered by decreasing T1w:T2w, as are areas within each group. Scatter plots are shown for T1w:T2w (horizontal axis) versus: **C** cytoarchitecture type (24), **D** Relative density of PV:(PV+SST) cells in L2/3 (19), **E** Sum of incoming inter-areal axonal projection weight (20), and **F** Inferred hierarchical level inferred from feedforward–feedback laminar projection patterns (13). Circles are colored according to the connectivity modules in **B** and have sizes scaled by T1w:T2w. A small amount of vertical noise has been added to points in **C** to aid visualization (cytoarchitecture type is discrete).

a decreasing trend from primary unimodal through to transmodal areas in macaque and human (11). T1w:T2w is not significantly correlated to variation in cell density (26), $\rho = 0.21$ ($p = 0.2$) nor neuron density, $\rho = 0.20$ ($p = 0.5$; for sixteen cortical areas of the Franklin and Paxinos atlas matched manually to the ARA (25), cf. Table S1), making it well positioned to capture density independent differences in neural architecture (8).

Cortical hierarchy varies with laminar differentiation, with primary somatosensory areas being the most clearly differentiated (10). T1w:T2w captures this variation, being positively correlated with cortical granularity in macaque, $\tau = 0.87$ (across eight cytoarchitectonic types) and human, $\rho = 0.74$ (using layer IV gene markers) (11). As shown in Fig. 1C, T1w:T2w also increases from dysgranular to eulaminar areas in mouse cortex, Kendall's $\tau = 0.51$ ($p = 2 \times 10^{-6}$, using five cytoarchitectonic categories assigned to 38 matching cortical areas (24)).

Relative interneuron densities vary continuous across mouse cortical areas (19). In layer 2/3, sensory-motor areas contain a greater proportion of (output-modulating) parvalbumin-containing (PV) interneurons, while association and frontal areas contain a greater proportion of (input-modulating) somatostatin-containing (SST) interneurons; the ratio $\mathrm{PV}/(\mathrm{PV}+\mathrm{SST})$ orders cortical areas along a candidate functional hierarchy (19). We computed the correlation between T1w:T2w and layer 2/3 density of each of three measured interneuron cell types: PV, SST, and vasoactive intestinal peptide-containing (VIP) cells, as well as the proposed hierarchy marker, the ratio PV:(PV+SST), across 36 matching cortical areas. PV:(PV+SST) is positively correlated with T1w:T2w, $\rho = 0.58$ ($p_{\mathrm{corr}} = 5 \times 10^{-4}$, correcting for four independent comparisons (33)), as shown in Fig. 1D. This trend is consistent with more functionally integrative areas (lower T1w:T2w) requiring a greater relative density of input-modulating SST to output-modulating PV interneurons.

We next investigated whether T1w:T2w is related to properties of interareal axonal connectivity, measured using viral tract tracing (20), focusing on the normalized axonal connection density projected to (weighted in-degree, k^w_{in}) and from (weighted out-degree, k^w_{out}) each cortical area. Across 38 matching areas, T1w:T2w is significantly correlated with k^w_{in}, $\rho = -0.40$ ($p_{\mathrm{corr}} = 0.03$, correcting for two independent comparisons (33)), plotted in Fig. 1E, but not with k^w_{out}, $\rho = 0.14$ ($p_{\mathrm{corr}} = 0.4$). This trend suggests that more functionally integrative areas (lower T1w:T2w) have a greater aggregate strength of axonal inputs.

Comprehensive data on laminar specific intracortical projection patterns have recently been used to assign candidate hierarchical levels to cortical areas (13). The mouse cortex does not fit neatly into a global structural hierarchy, with a hierarchy score of just 0.126 (where 0 is non-hierarchical and 1 is perfectly hierarchical) (13). T1w:T2w and inferred hierarchical level are strongly negatively correlated in macaque, $\rho = -0.76$ (11), but only weakly negatively correlated in mouse, $\rho = -0.29$ ($p = 0.09$), as shown in Fig. 1F. Structural hierarchical organization of the cortex exhibits a much stronger relationship with T1w:T2w in macaque than in mouse.

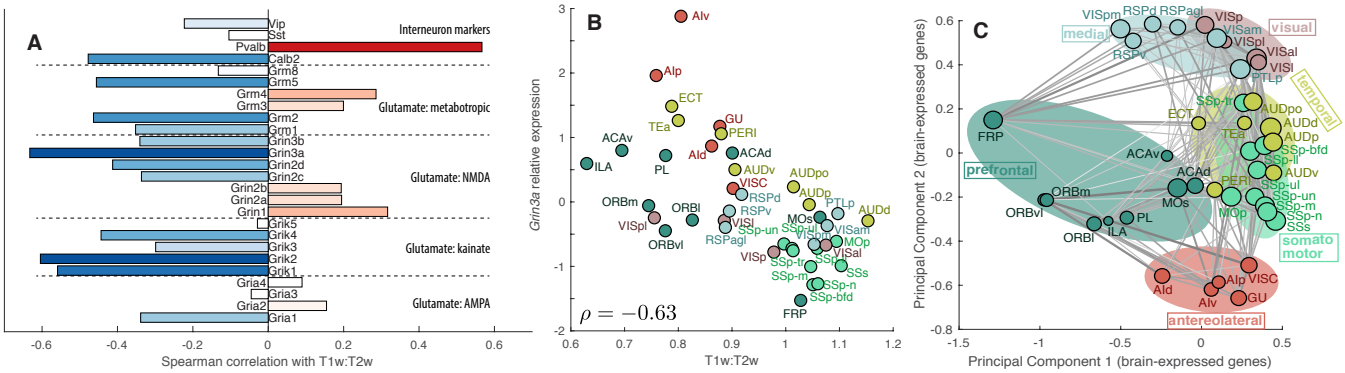

Fig. 2. Transcriptional maps of some key receptor subunit and cell-type marker genes covary with the T1w:T2w map, and brain-expressed genes together organize cortical areas into meaningful processing streams. **A** Spearman correlation coefficients, ρ, between T1w:T2w and the transcriptional maps of genes coding glutamate receptor subunits and interneuron cell-type markers. **B** Scatter plot of T1w:T2w versus z-score normalized transcriptional levels of *Grin3a*, $\rho = -0.63$ ($p_{\text{corr}} = 5 \times 10^{-4}$). **C** Projection of brain areas into the space of the two leading principal components of 1055 brain-expressed genes (34) places cortical areas with similar transcriptional profiles close in the space and organizes the cortex into functionally relevant groupings. Brain areas are shown as circles with radii scaled by T1w:T2w and (symmetrized) axonal projections (20) are annotated where possible.

Gene transcriptional gradients. Gene transcriptional maps of the mouse brain, measured with cellular resolution using *in situ* hybridization, form the Allen Mouse Brain Atlas (AMBA) (18). We developed and applied stringent quality criteria to obtain spatial transcriptional maps of 4181 genes (see Supporting Information). We first focus on a selected set of 86 receptor subunit and cell-type marker genes (5) (see Supporting Information). After correcting for testing multiple independent hypotheses (33) (a conservative correction due to the high intercorrelation between many of these genes), we found that 24 genes display transcriptional maps that are significantly correlated with T1w:T2w ($p_{\text{corr}} < 0.05$; $|\rho| \geq 0.39$), ranging from glutamate receptor subunits (*Grin3a*, *Grin2d*, *Grik1*, *Grik2*, *Grik4*, *Grm2*, *Grm5*); serotonin receptor subunits (*Htr1a*, *Htr2c*, and *Htr5b*); interneuron cell-type markers (*Pvalb* and *Calb2*); the myelin marker, *Mobp*; and a range of other receptor subunit genes: *Trhr*, *Mc4r*, *Chrm5*, *Galr2*, *Hcrtr2*, *Hcrtr1*, *P2ry12*, *P2ry14*, *Cnr1*, *Oxtr*, *P2ry2* (see Table S2 for full list). Correlations between T1w:T2w and transcriptional levels of a selected subset of glutamate receptor subunit and interneuron marker genes are plotted in Fig. 2A. The strong negative correlation between T1w:T2w and *Grin3a* expression, $\rho = -0.63$ ($p_{\text{corr}} = 5 \times 10^{-4}$), is plotted in Fig. 2B.

To understand how T1w:T2w relates to dominant transcriptional gradients of brain-expressed genes (a set of 1055 genes (34)), we used principal components analysis (PCA) to estimate the most explanatory spatial maps of transcriptional variation (accounting for missing values using probabilistic PCA (36), see Supporting Information). The first PC of cortical transcription is significantly correlated with the T1w:T2w map, $|\rho| = 0.53$ ($p = 6 \times 10^{-4}$), as it is in human cortex, $|\rho| = 0.81$ (11) (the correlation with PC2 is weaker, $|\rho| = 0.29$, cf. Fig. S2). Figure 2C displays a projection of cortical areas into the space of the two leading PCs, placing areas with similar transcriptional profiles close to one another in the space. This transcriptional organization of mouse cortical areas clearly separates different functional processing streams and visually resembles parallel primary–transmodal hierarchies (10) that have recently been characterized in human rs-fMRI (6).

Laminar specificity. Are large-scale cortical gradients driven by the specialization of specific cortical layers? We investigated this question in mouse using layer-specific maps of gene transcription (18) and interneuron density (19). T1w:T2w was estimated for each brain area by combining all cortical layers (values of T1w:T2w computed in layers 1–5 were highly correlated to this overall measurement, see Fig. S3).

We first computed Spearman correlation coefficients, ρ, between T1w:T2w and three interneuron cell densities (19) in each of five cortical layers: 1 (37 areas), 2/3 (37 areas), 4 (21 areas), 5 (36 areas), and 6 (35 areas). Results are plotted in Fig. 3A for each cortical layer (row) and cell type (column). Correcting across 15 (assumed independent) hypothesis tests (33)—each cell type in each cortical layer—we found a significant positive correlation between T1w:T2w and PV cell density in layer 5, $\rho = 0.52$ ($p_{\text{corr}} = 7 \times 10^{-3}$), and a negative correlation of SST cell density with T1w:T2w in layer 2/3, $\rho = -0.62$ ($p_{\text{corr}} = 4 \times 10^{-4}$) and layer 6, $\rho = -0.65$ ($p_{\text{corr}} = 4 \times 10^{-4}$). VIP cell density did not exhibit a significant correlation to T1w:T2w in any individual cortical layer.

We next investigated gene expression patterns in cortical layers 1, 2/3, 4, 5, 6a, and 6b (18) across the 24 genes identified above to be significantly correlated to T1w:T2w, shown in Fig. 3B (results for all 86 genes are in Fig. S4). Consistent with *Pvalb* expression as a marker of PV cell density, the two measurements exhibit a very similar laminar pattern of T1w:T2w correlations (with the strongest correlation in layer 5, cf. Fig. 3A). For a given gene, the direction of correlation between T1w:T2w and gene expression is generally consistent across cortical layers. Some genes display an association with T1w:T2w in all individual layers (e.g., *Trhr*, *Grin3a*, and *Htr2c*), while other genes show an overall correlation with T1w:T2w that is restricted to specific cortical layers (e.g., the positive correlation with *Mobp* is driven by layer 4 and infragranular layers). These results demonstrate that

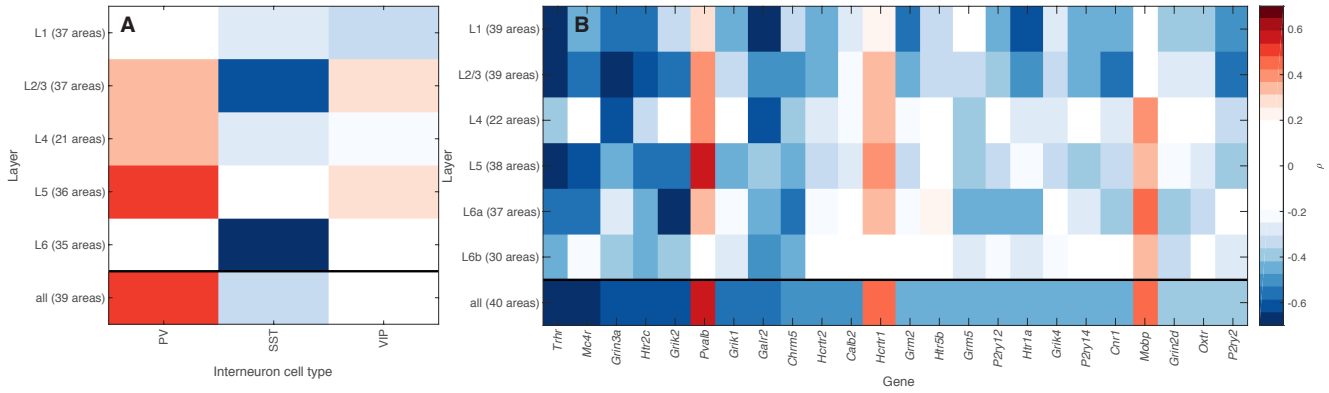

Fig. 3. Cell densities and gene expression exhibit distinctive laminar patterns of covariation with T1w:T2w across the mouse cortex. Spearman correlation coefficients, ρ, of T1w:T2w are plotted as color for: **A** cell density of three types of interneurons (19), and **B** transcriptional level of a given gene (column) in a given cortical layer (row). Overall correlations, obtained from combining all layers of each area, are shown in the bottom row of each plot. Transcriptional levels (18) are shown for the 24 genes with significant overall correlations to T1w:T2w, ordered by their overall correlation to T1w:T2w (results for all 86 brain-related genes are in Fig. S4).

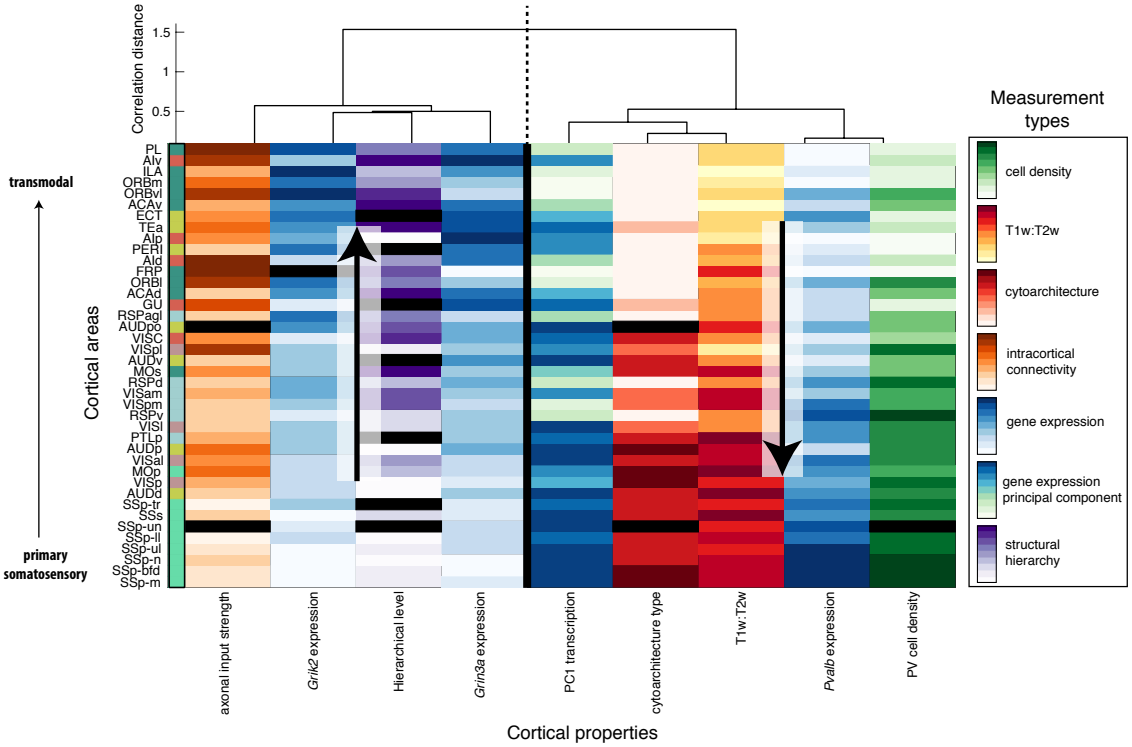

Fig. 4. Diverse independent measurements of microstructure display a common broad gradient of variation across cortical areas. Cortical areas form rows, and measurements form columns, with different color maps used to code different datasets(from low values, light, to high values, dark), as labeled: density of PV neurons (19) (green), T1w:T2w (35) (yellow/red), cytoarchitecture (24) (red), weighted in-degree, k^w, of normalized axonal projection density (20) (orange), expression of three selected genes: *Grin3a*, *Grik2*, and *Pvalb* (18) (blue) and the first principal component of brain-related genes (green-blue), and estimated hierarchical level (13) (purple). Areas (rows) are ordered according to the first principal component of this multimodal matrix of cortical properties and are colored according to their membership to one of six connectivity-based groupings (13) (cf. Fig. 1B). Measurements (columns) are ordered according to average linkage clustering on correlation distances according to the annotated dendrogram. Measurements cluster into two groups that either increase (left cluster) or decrease (right cluster) along a candidate functional hierarchy, from primary somatosensory through to transmodal prefrontal areas. Missing data are shown as black rectangles.

macroscopic gradients of areal specialization are not dominated by gene transcription in particular cortical layers; all layers exhibit macroscopic gradients of areal specialization, for distinct microcircuit properties.

A common hierarchical gradient. The variation of T1w:T2w appears to mirror the large-scale variation of cortical microstructure along a putative functional hierarchy. To more directly understand relationships between diverse mouse cortical gradients characterized above, we combined representative measurements from each data type: gene expression, intracortical axonal connectivity, T1w:T2w, and interneuron cell density. These properties were visualized together by plotting the cortical variation of each measurement type with a distinct color map, as shown in Fig. 4. Measurements (columns) with highly correlated variation across cortical areas (rows) were placed close to each other using linkage clustering (see Supporting Information). A common gradient emerges from the covariation of these diverse measurements of cortical structure, estimated as the first princi-

pal component of the data and used to reorder the rows of Fig. 4. This consensus gradient orders areas along a putative functional hierarchy, from primary somatosensory through to integrative prefrontal areas. Each individual measurement either increases or decreases along this consensus gradient, forming the two anticorrelated clusters shown in Fig. 4.

To investigate whether ordering areas by T1w:T2w or by the structural hierarchical ordering of Harris et al. (13) better explains the multimodal cortical gradients, we compared how each correlates with the properties shown in Fig. 4 (across the 35 cortical areas common to both measurements). Spearman correlation coefficients were similar in magnitude between T1w:T2w and hierarchical level, and all but one property (PV cell density) were more strongly correlated with T1w:T2w than with hierarchical level (see Fig. S5).

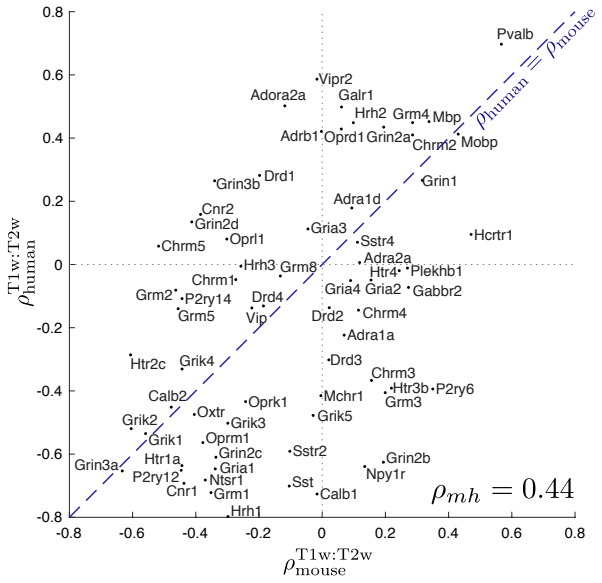

Fig. 5. Mouse–human consistency of T1w:T2w and transcriptional gradients of brain-related genes. We plot the correlation between T1w:T2w and transcription levels in mouse, $\rho^{\text{T1w:T2w}}_{\text{mouse}}$ (horizontal axis) and human, $\rho^{\text{T1w:T2w}}_{\text{human}}$ (vertical axis) for 70 brain-related genes. The equality line, $\rho_m = \rho_h$, is shown dashed blue. Transcriptional maps of key brain-related genes vary similarly with T1w:T2w in mouse and human cortex, $\rho_{mh} = 0.44$ ($p = 1 \times 10^{-4}$).

Mouse–human consistency between T1w:T2w and gene transcriptional gradients. T1w:T2w follows dominant transcriptional gradients in mouse and human cortex (11), but are the gradients of specific brain-related genes conserved between the two species? To investigate this, we compared the correlation between T1w:T2w and the transcription map of a given gene in mouse cortex, ρ_m, and for the human ortholog of that gene in human cortex, ρ_h (11), repeating the calculation the 70 of our 86 brain-related genes analyzed that have human orthologs (and could be matched to human data (11)). Interspecies consistency in transcriptional gradients is reflected by a correspondence between ρ_m and ρ_h, which we measured as the correlation (of ρ_m and ρ_h) across genes, denoted as ρ_{mh}. Despite high genome coverage, the AMBA (18) and Allen Human Brain Atlas (AHBA) (37) can be noisy at level of individual experiments; although we have been careful to process and apply rigorous quality control criteria, weak correlations in either human (low ρ_h) or mouse (low ρ_m) should not be interpreted as an absence of a relationship with T1w:T2w as much as strong correlations can be interpreted as evidence for a relationship.

As shown in Fig. 5, we find significant interspecies correspondence, $\rho_{mh} = 0.44$ ($p = 1 \times 10^{-4}$). The agreement is striking given measurement noise, vast differences in spatial scale, and distinct measurement modalities between mouse (high-throughput *in situ* hybridization) and human (post-mortem microarray from six adults). Two of the genes with the strongest correlations with T1w:T2w in mouse cortex exhibit a similar variation in human cortex: *Grin3a/GRIN3A* ($\rho_m = -0.63$, $\rho_h = -0.65$) and *Pvalb/PVALB* ($0.57, 0.70$). A range of other key genes exhibit strong interspecies consistency, including the interneuron marker *Calb2* ($-0.48, -0.45$), the oxytosin receptor gene, *Oxtr* ($-0.41, -0.48$), glutamate receptor genes *Grik1* ($-0.56, -0.54$), *Grik2* ($-0.60, -0.52$), and *Grik4* ($-0.44, -0.33$), and myelin marker genes *Mobp* ($0.43, 0.41$) and *Mbp* ($0.34, 0.45$). Significant mouse–human correspondence was not limited to the brain-related genes shown in Fig. 5, but was reproduced for: (i) all 2951 genes, $\rho_{mh} = 0.25$ ($p = 8 \times 10^{-42}$); (ii) 806 brain-expressed genes (34), $\rho_{mh} = 0.31$ ($p = 2 \times 10^{-19}$); (iii) 60 astrocyte-enriched genes, $\rho_{mh} = 0.38$ ($p = 3 \times 10^{-3}$); (iv) 143 neuron-enriched genes, $\rho_{mh} = 0.40$ ($p = 6 \times 10^{-7}$); and (v) 41 ogligodendrocyte-enriched genes, $\rho_{mh} = 0.65$ ($p = 7 \times 10^{-6}$) (38). Mouse–human correspondence increased as progressively more stringent quality control criteria were applied to the data, consistent with an enhancement of meaningful signal (see Fig. S6).

Discussion

Macroscale spatial variations in the makeup of a canonical cortical circuit (39, 40)—its cell types and their interconnectivity, synaptic receptors, and cyto- and myeloarchitecture (1, 3, 41)—may reflect a biological substrate of functional specialization that enables efficient processing and integration of diverse sensory information (7, 11) across multiple timescales (42–44). Circumventing the need to define interspecies homologies, here we used the noninvasive MRI contrast map, T1w:T2w, as a common reference for interspecies comparison, demonstrating that large-scale gradients in macaque and human cortex (11) qualitatively match those in mouse, which displays an under-appreciated level of interareal heterogeneity. Specifically, T1w:T2w broadly decreases from primary sensory to multimodal areas, with high T1w:T2w associated with a eulaminar cytoarchitecture. The dominant map of transcriptional variation (estimated using PCA) is significantly correlated with T1w:T2w in both mouse and human, and the transcriptional maps of genes encoding major synaptic receptors and neuronal cell types vary similarly between mouse and human cortex. Using high-resolution invasive measurements available in mouse, we report new connections between T1w:T2w and interneuron densities, laminar-specific gene expression, and interareal axonal connectivity. Our results suggest the existence of a fundamental architectural machinery underlying stereotypical

hierarchical function. For example, low T1w:T2w indexes the integrative function of multimodal areas, and this function may be supported a greater density of input-modulating PV interneurons, a greater density of NMDA subunit 3A glutamate receptor subunits (*Grin3a*), and a greater relative strength of incoming axonal projections. While the full complexity of cortical diversity clearly cannot be captured along a single spatial dimension, the covariation of diverse aspects of microcircuit architecture along a common spatial map, and its interspecies correspondence, supports the existence of a conserved architectural scaffold supporting hierarchical specialization in mammalian brains.

While anatomical comparisons of rodent and primate brains have been relatively sparse to date, they have uncovered key interspecies differences. For example, in rhesus monkey, the physiology and morphology of layer 3 pyramidal neurons (14) and glutamatergic synaptic structure (15) show strong interareal differences between V1 and frontal cortex, properties that are strikingly homogeneous by comparison between homologous areas of mouse cortex. A relative increase in cortical heterogeneity in primate has also been observed in the more pronounced rostro-caudal gradients of neurogenesis, and resulting variations in adult neuron density (8, 45, 46). While the mouse cortex exhibits hierarchical feedforward-feedback projection patterns in specific (e.g., visual) processing streams (47), with corresponding variation in microstructure (48), interareal laminar projections across the whole cortex are far more stereotyped in macaque (12) than mouse (13). The mouse cortex also appears to fit only weakly into a global hierarchical organization, attaining a hierarchy score of just 0.126 (where a score of 1 corresponds to an ideal hierarchy (13)), although this index is yet to be calculated in macaque, preventing direct interspecies comparison.

As well as substantial differences, our results highlight a previously underappreciated spatial dimension of mouse cortical specialization and establish a commonality with human cortical specialization. The consistency of transcriptional maps of 70 receptor subunit and cell-type marker genes with the common reference map, T1w:T2w, in mouse and human ($\rho_{mh} = 0.44$, $p = 1 \times 10^{-4}$) is striking given vastly different spatial scales and major differences in expression measurement between mouse (high-throughput *in situ* hybridization (18)) and human (microarray data from six post-mortem subjects (37)). A two-dimensional projection of mouse cortical areas based on their transcriptional signatures across brain-expressed genes (Fig. 2C), distinguishes somatomotor, auditory, and visual processing streams from anteriolateral and prefrontal areas, analagous to how parallel processing streams are represented in low-dimensional embeddings of human fMRI correlation networks (6, 49). However, despite qualitative interspecies consistencies, correlations with T1w:T2w are generally weaker in mouse than primate. For example, T1w:T2w correlates strongly with hierarchical level in macaque ($\rho = -0.76$) but only weakly in mouse ($\rho = -0.29$). Correlations of T1w:T2w with cytoarchitectural type ($\tau_{\text{mouse}} = 0.51$, $\tau_{\text{macaque}} = 0.87$), and the leading principal component spatial map of gene transcription ($|\rho_{\text{mouse}}| = 0.53$, $|\rho_{\text{human}}| = 0.81$) (11) are also weaker in mouse, consistent with a lesser degree of hierarchical functional specialization relative to primate. Species-specific deviations from a prototypical anatomical substrate for hierarchical information processing may be the result of evolutionary selection, and are also likely to be contributed to by a larger brain size and a prolonged developmental schedule (both in absolute duration and as a proportion of the developmental period) in primate (8, 45, 46, 50).

T1w:T2w is commonly interpreted as a marker of gray-matter myelin content (51), although both T1- and T2-weighted images are sensitive to a wide range of microstructural properties (52). Our results provide transcriptional evidence for a connection between T1w:T2w and myelin, demonstrating a significant relationship with the expression of *Mobp* and other oligodendrocyte-enriched genes (which also display high mouse–human correspondence; see Supporting Information). Axonal myelination improves transmission speeds (53) and prevents the formation of new synaptic connections (54, 55), properties that are broadly consistent with fast, 'hard-wired' computations in heavily myelinated somatosensory areas relative to more plastic and adpative prefrontal areas. However, while some gradients, such as the covariation of T1w:T2w with heavily myelinated PV interneurons (53, 56), can be plausibly linked to relative myelination levels, many others cannot (such as the transcriptional maps of *Grin3a* and *Calb2*). This suggests that the convergence of multimodal cortical gradients may reflect deeper organizational mechanisms acting in concert, perhaps through development (32).

As more is learned about how variations in cellular and synaptic microstructure shape functional specialization in the cortex, it will be important to complement this understanding with new mathematical models of brain dynamics that are properly constrained by the breadth and spatial detail of new datasets (19, 43, 57, 58). Insights from this common structure, interpreting each cortical area as a local computational unit (39), may also aid motivation for the next generation of brain-inspired machine learning algorithms (59). Such approaches will allow theory and experiment to develop in tandem, with physiologically-constrained mathematical models making functional predictions that can be tested experimentally and used to refine the models. Our findings offer guidance for the development of dynamical and functional models of large-scale cortical circuits in mouse, monkey, and human.

ACKNOWLEDGEMENTS

We would like to thank Alex Fornito for his detailed and insightful comments on the manuscript. B.D.F is supported by the National Health and Medical Research Council 1089718. J.D.M. is supported by NIMH grant R01 MH112746. V.Z. is supported by the SNSF AMBIZIONE PZ00P3_173984. X.J.W. is supported by NIMH grant R01MH062349, Simons Collaborative Global Brain (SCGB) Program Grant 543057SPI, and STCSM grant 15JC1400104.

References

1. N. Palomero-Gallagher and K. Zilles. Cortical layers: Cyto-, myelo-, receptor- and synaptic architecture in human cortical areas. *NeuroImage* (2017).
2. M. P. van den Heuvel and B. T. T. Yeo. A Spotlight on Bridging Microscale and Macroscale Human Brain Architecture. *Neuron* **93**, 1248 (2017).
3. A. Paul, M. Crow, R. Raudales, et al. Transcriptional Architecture of Synaptic Communication Delineates GABAergic Neuron Identity. *Cell* **171**, 522 (2017).

4. L. H. Scholtens, R. Schmidt, M. A. de Reus, and M. P. van den Heuvel. Linking Macroscale Graph Analytical Organization to Microscale Neuroarchitectonics in the Macaque Connectome. *J. Neurosci.* **34**, 12192 (2014).
5. S. Janušonis. A receptor-based analysis of local ecosystems in the human brain. *BMC Neurosci.* **18**, 551 (2017).
6. D. S. Margulies, S. S. Ghosh, A. Goulas, et al. Situating the default-mode network along a principal gradient of macroscale cortical organization. *Proc. Natl. Acad. Sci. USA* **113**, 12574 (2016).
7. J. M. Huntenburg, P.-L. Bazin, P. L. Bazin, and D. S. Margulies. Large-Scale Gradients in Human Cortical Organization. *TICS* **22**, 21 (2017).
8. C. J. Charvet and B. L. Finlay. Evo-Devo and the Primate Isocortex: The Central Organizing Role of Intrinsic Gradients of Neurogenesis. *Brain Behav. Evol.* **84**, 81 (2014).
9. K. Wagstyl, L. Ronan, I. M. Goodyer, and P. C. Fletcher. Cortical thickness gradients in structural hierarchies. *NeuroImage* **111**, 241 (2015).
10. M. M. Mesulam. From sensation to cognition. *Brain* **121**, 1013 (1998).
11. J. B. Burt, M. Demirtas, W. J. Eckner, et al. Hierarchy of transcriptomic specialization across human cortex captured by structural neuroimaging topography. *Nat. Neurosci.* **27** (2018).
12. N. T. Markov, M. Ercsey-Ravasz, A. R. R. Gomes, et al. A Weighted and Directed Interareal Connectivity Matrix for Macaque Cerebral Cortex. *Cereb. Cortex* **24**, 17 (2012).
13. J. A. Harris, S. Mihalas, K. E. Hirokawa, et al. The organization of intracortical connections by layer and cell class in the mouse brain. *bioRxiv* p. 292961 (2018).
14. J. P. Gilman, M. Medalla, and J. I. Luebke. Area-Specific Features of Pyramidal Neurons—a Comparative Study in Mouse and Rhesus Monkey. *Cereb. Cortex* **27**, 2078 (2016).
15. A. Hsu, J. I. Luebke, and M. Medalla. Comparative ultrastructural features of excitatory synapses in the visual and frontal cortices of the adult mouse and monkey. *J. Comparat. Neurol.* **525**, 2175 (2017).
16. J. I. Luebke. Pyramidal Neurons Are Not Generalizable Building Blocks of Cortical Networks. *Front. Neuroanat.* **11**, 13644 (2017).
17. D. Fürth, T. Vaissière, O. Tzortzi, et al. An interactive framework for whole-brain maps at cellular resolution. *Nat. Neurosci.* **21**, 139 (2017).
18. E. Lein, M. J. Hawrylycz, N. Ao, et al. Genome-wide atlas of gene expression in the adult mouse brain. *Nature* **445**, 168 (2006).
19. Y. Kim, G. R. Yang, K. Pradhan, et al. Brain-wide Maps Reveal Stereotyped Cell-Type-Based Cortical Architecture and Subcortical Sexual Dimorphism. *Cell* **171**, 456 (2017).
20. S. W. Oh, J. A. Harris, L. Ng, et al. A mesoscale connectome of the mouse brain. *Nature* **508**, 207 (2014).
21. B. Zingg, H. Hintiryan, L. Gou, et al. Neural Networks of the Mouse Neocortex. *Cell* **156**, 1096 (2014).
22. H. Hintiryan, N. N. Foster, I. Bowman, et al. The mouse cortico-striatal projectome. *Nat. Neurosci.* **19**, 1100 (2016).
23. R. Gămănuț, H. Kennedy, Z. Toroczkai, et al. The Mouse Cortical Connectome, Characterized by an Ultra-Dense Cortical Graph, Maintains Specificity by Distinct Connectivity Profiles. *Neuron* **97**, 698 (2018).
24. A. Goulas, H. B. M. Uylings, and C. C. Hilgetag. Principles of ipsilateral and contralateral cortico-cortical connectivity in the mouse. *Brain. Struct. Funct.* **252**, 1 (2016).
25. S. Herculano-Houzel, C. R. Watson, and G. Paxinos. Distribution of neurons in functional areas of the mouse cerebral cortex reveals quantitatively different cortical zones. *Front. Neuroanat.* **7**, 35 (2013).
26. T. C. Murakami, T. Mano, S. Saikawa, et al. A three-dimensional single-cell-resolution whole-brain atlas using CUBIC-X expansion microscopy and tissue clearing. *Nat. Neurosci.* **21**, 625 (2018).
27. V. Zerbi, J. Grandjean, M. Rudin, and N. Wenderoth. Mapping the mouse brain with rs-fMRI: An optimized pipeline for functional network identification. *NeuroImage* **123**, 11 (2015).
28. S. S. Sethi, V. Zerbi, N. Wenderoth, A. Fornito, and B. D. Fulcher. Structural connectome topology relates to regional BOLD signal dynamics in the mouse brain. *Chaos* **27**, 047405 (2017).
29. J. Grandjean, V. Zerbi, J. Balsters, N. Wenderoth, and M. Rudina. The structural basis of large-scale functional connectivity in the mouse. *J. Neurosci.* **37**, 0438 (2017).
30. B. D. Fulcher and A. Fornito. A transcriptional signature of hub connectivity in the mouse connectome. *Proc. Natl. Acad. Sci. USA* **113**, 1435 (2016).
31. H.-W. Dong. *The Allen reference atlas: A digital color brain atlas of the C57Bl/6J male mouse.* John Wiley & Sons Inc., Hoboken, NJ, US (2008).
32. T. Chomiak and B. Hu. Mechanisms of Hierarchical Cortical Maturation. *Front. Cell. Neurosci.* **11**, 150 (2017).
33. Y. Benjamini and Y. Hochberg. Controlling the False Discovery Rate: A Practical and Powerful Approach to Multiple Testing. *J. Roy. Stat. Soc. B* **57**, 289 (1995).
34. J. H. Finger, C. M. Smith, T. F. Hayamizu, et al. The mouse Gene Expression Database (GXD): 2017 update. *Nucl. Acid. Res.* **45**, D730 (2017).
35. R. Bakker, P. Tiesinga, and R. Kötter. The Scalable Brain Atlas: Instant Web-Based Access to Public Brain Atlases and Related Content. *NeuroInf.* **13**, 353 (2015).
36. A. Ilin and T. Raiko. Practical Approaches to Principal Component Analysis in the Presence of Missing Values. *J. Mach. Learn. Res.* **11**, 1957 (2010).
37. M. J. Hawrylycz, E. Lein, A. L. Guillozet-Bongaarts, et al. An anatomically comprehensive atlas of the adult human brain transcriptome. *Nature* **489**, 391 (2012).
38. J. D. Cahoy, B. Emery, A. Kaushal, et al. A transcriptome database for astrocytes, neurons, and oligodendrocytes: a new resource for understanding brain development and function. *J. Neurosci.* **28**, 264 (2008).
39. R. J. Douglas and K. A. C. Martin. Mapping the Matrix: The Ways of Neocortex. *Neuron* **56**, 226 (2007).
40. K. D. Harris and G. M. G. Shepherd. The neocortical circuit: themes and variations. *Nat. Neurosci.* **18**, 170 (2015).
41. K. Zilles and N. Palomero-Gallagher. Multiple Transmitter Receptors in Regions and Layers of the Human Cerebral Cortex. *Front. Neuroanat.* **11**, 78 (2017).
42. J. D. Murray, A. Bernacchia, D. J. Freedman, et al. A hierarchy of intrinsic timescales across primate cortex. *Nat. Neurosci.* **17**, 1661 (2014).
43. R. Chaudhuri, K. Knoblauch, M.-A. Gariel, H. Kennedy, and X.-J. Wang. A Large-Scale Circuit Mechanism for Hierarchical Dynamical Processing in the Primate Cortex. *Neuron* **88**, 419 (2015).
44. R. Duarte, A. Seeholzer, K. Zilles, and A. Morrison. Synaptic patterning and the timescales of cortical dynamics. *Curr. Opin. Neurobiol.* **43**, 156 (2017).
45. D. J. Cahalane, C. J. Charvet, and B. L. Finlay. Modeling local and cross-species neuron number variations in the cerebral cortex as arising from a common mechanism. *Proc. Natl. Acad. Sci. USA* **111**, 17642 (2014).
46. C. J. Charvet, D. J. Cahalane, and B. L. Finlay. Systematic, Cross-Cortex Variation in Neuron Numbers in Rodents and Primates. *Cereb. Cortex* **25**, 147 (2015).
47. R. D. D'Souza and A. Burkhalter. A Laminar Organization for Selective Cortico-Cortical Communication. *Front. Neuroanat.* **11**, 411 (2017).
48. R. D. D'Souza, A. M. Meier, P. Bista, Q. Wang, and A. Burkhalter. Recruitment of inhibition and excitation across mouse visual cortex depends on the hierarchy of interconnecting areas. *eLife* **5**, 1025 (2016).
49. X. Guell, J. D. Schmahmann, J. D. Gabrieli, and S. S. Ghosh. Functional gradients of the cerebellum. *eLife* **7**, 568 (2018).
50. R. L. Buckner and F. M. Krienen. The evolution of distributed association networks in the human brain. *Trends in Cognitive Sciences* **17**, 648 (2013).
51. M. F. Glasser and D. C. Van Essen. Mapping Human Cortical Areas In Vivo Based on Myelin Content as Revealed by T1- and T2-Weighted MRI. *J. Neurosci.* **31**, 11597 (2011).
52. S. Lorio, F. Kherif, A. Ruef, et al. Neurobiological origin of spurious brain morphological changes: A quantitative MRI study. *Hum. Brain Map.* **37**, 1801 (2016).
53. K. D. Micheva, D. Wolman, B. D. Mensh, et al. A large fraction of neocortical myelin ensheathes axons of local inhibitory neurons. *eLife* **5**, e15784 (2016).
54. V. Braitenberg. A note on myeloarchitectonics. *J. Comparat. Neurol.* **118**, 141 (1962).
55. J. M. Huntenburg, P.-L. Bazin, A. Goulas, et al. A Systematic Relationship Between Functional Connectivity and Intracortical Myelin in the Human Cerebral Cortex. *Cereb. Cortex* **27**, 981 (2017).
56. J. Stedehouder, J. J. Couey, D. Brizee, et al. Fast-spiking Parvalbumin Interneurons are Frequently Myelinated in the Cerebral Cortex of Mice and Humans. *Cereb. Cortex* **27**, 5001 (2017).
57. M. Demirtas, J. B. Burt, M. Helmer, et al. Hierarchical heterogeneity across human cortex shapes large-scale neural dynamics. *bioRxiv* p. 341966 (2018).
58. J. D. Murray, M. Demirtas, and A. Anticevic. Biophysical modeling of large-scale brain dynamics and applications for computational psychiatry. *Biol. Psychiatry: Cog. Neurosci. Neuroimag.* (2018).
59. A. H. Marblestone, G. Wayne, and K. P. Kording. Toward an Integration of Deep Learning and Neuroscience. *Front. Comput. Neurosci.* **10**, 406 (2016).